Finite Element Method (FEM) Study on Space Charge Effects in Organic Light Emitting Diodes (OLED)

Kwang-sik Kim, Young-Wook Hwang, and Tae-Young Won

Abstract— **In this paper, we present a finite element method (FEM) study on the space charge effects in organic light emitting diodes. The physical model covers all the key physical processes in OLEDs, namely charge injection, transport and recombination, exciton diffusion, transfer and decay as well as light coupling, and thin-film-optics. The exciton model includes generation, diffusion, and energy transfer as well as annihilation. We assumed that the light emission originates from oscillation which thus is embodied as exciton in a stack of multilayer. We discuss the accumulation of charges at internal interfaces and their signature in the transient response as well as the electric field distribution. We also report our investigation on the influence of the insertion of the emission layer (EML) in the bilayer structure.**

Index Terms—**Organic light emitting diodes (OLEDs), finite element method (FEM)**

I. INTRODUCTION

In order to improve the electrical and optical properties of the OLED, we need to develop a numerical engineering tool. We developed a numerical engineering tool for the optimization of the multilayer device structure which is basically composed of an organic electroluminescent layer sandwiched by two metal electrodes. In this work, we present a finite element method (FEM) study of space charge effects in organic light emitting diodes and numerical framework of Ref. [1]. Our model includes a Gaussian density of states to account for the energetic disorder in organic semiconductors and the Fermi-Dirac statistics to account for the charge hopping process between uncorrelated sites. The physical model covers all the key physical processes in OLEDs, namely charge injection, transport and recombination, exciton diffusion, transfer and decay as well as light coupling, and thin-film-optics. The exciton model includes generation, diffusion, and energy transfer as well as annihilation. We assumed that the light emission originates from oscillating and thus embodied as excitons and embedded in a stack of multilayer. The out-coupled emission spectrum has been numerically calculated as a function of viewing angle, polarization, and dipole orientation. We discuss the accumulation of charges at internal interfaces and their signature in the transient response as well as the electric field distribution.

II. NUMERICAL MODEL

General semiconductor drift-diffusion equations for electrons and holes are employed for the description of charge transport in OLED. The carrier densities in Poisson equation consist of mobile charge carriers as well as trapped charges. The current density consists of a drift part caused by the electric field and diffusion current. We assumed that the mobility is dependent on the electric field and temperature. We utilized a Gaussian density of states (DOS) to account for the disorder of the organic materials which is caused by molecular structure [1, 3, 5]. The governing equations for OLED devices are

Manuscript received Apr. 30, 2012; revised Sep. 4, 2012.
Graduate School of Electrical Engineering, Inha University 253 Yonghyun-dong Nam-ku, Incheon, Korea 402-751
E-mail : {kks, hyw, twon}@hsel.inha.ac.kr

written as:

$$\frac{\partial E(x)}{\partial x} = \frac{q}{\varepsilon}(p(x) - n(x)) \quad (1)$$

$$J_n(x) = q\mu_n n(x)E(x) + D_n \frac{\partial n(x)}{\partial x} \quad (2)$$

$$J_p(x) = q\mu_p p(x)E(x) + D_p \frac{\partial p(x)}{\partial x} \quad (3)$$

where n is the density of eletrons, p the density of holes, E the electric field, and ε the dielectric constant, q the elementary electric charge, and μ_n and μ_p are electron mobility and hole mobility, respectively. In Eqs. (2) and (3), D_n and D_p are electron diffusion constant and hole diffusion constant related by the Einstein relationship.

$$\frac{\partial n}{\partial t} = \frac{1}{q}\nabla J_n - R(n,p) - \frac{\partial n_t}{\partial t} \quad (4)$$

$$\frac{\partial p}{\partial t} = -\frac{1}{q}\nabla J_p - R(n,p) - \frac{\partial p_t}{\partial t} \quad (5)$$

Here, J_n and J_p are electron current density and hole current density, respectively. In addition, n_t and p_t represent trapped electron density and trapped hole density, respectively. Here, R represents bimolecular recombination rate. The trapped electron and holes obey the rate equations as the following:

$$\frac{\partial n_t}{\partial t} = r_c n(N_t - n_t) - r_e n_t \quad (6)$$

$$\frac{\partial p_t}{\partial t} = r_c p(N_t - p_t) - r_e p_t \quad (7)$$

where N_t is the trap density, r_c the capture rate, and r_e the emission rate. We also implemented the generation, transport and decay of excitons in the numerical tool. While electron-hole recombination may be locally confined, the resulting excitons are assumed to migrate with a characteristic diffusion constant before decaying radiatively or transferring their energy to other exciton species in the same layer. Thus, the rate equation S_i for exciton species contains a generation, a diffusion, transfer and non-radiative terms as the following:

$$\frac{\partial S_i}{\partial t} = G_i R + \vec{\nabla} J_{S_i} - (k_{rad_i} + k_{nonrad_i}) \cdot S_i$$

$$- k_{annihilation_i} \cdot S_i^2 + \sum_{j=1}^{n_{exc}} (k_{ji} \cdot S_j - k_{ij} \cdot S_i) \quad (8)$$

where G_i is a constant for generation efficiency, k_{rad_i} the radiative decay rate, k_{nonrad_i} the non-radiative decay rate and $k_{annihilation_i}$ an annihilation rate. We employed Forster and Dexter energy transfer mechanism which relies on the spectral overlap of the emission spectrum of the donating exciton species with the absorption spectrum of the accepting exciton species [4, 5]. The Scharfetter-Gummel method is used to spatially discretize the above equations and an iterative procedure was used to obtain the self- consistent solution.

III. Simulation Results

Fig. 1 is a schematic diagram illustrating the multilayer structure for organic light emitting diodes under this work. The device structure comprises a 2,2, 7,7 –tetrakis (N,N- dipheny -lamine)-9,9 -spirobi-fluorene (S-TAD) for hole transport layer (HTL), an 2,2, 7,7 –tetrakis (2,2-diphenylvinyl) spiro-9,9 -bifluorene (S-DPVBi) for the blue light emission, and an tris(8-hydroxyquinolinato)aluminum (Alq_3) for electron transport layer (ETL). The length of each layer is 50 nm, 15 nm, and 45 nm, respectively. The LUMO level is 2.6, 2.8 and 3.0 eV, and the HOMO level is 5.5, 5.6, and 5.7 eV in sequence [2]. We chose the electrode in such a way that the anode work function is 5.2 eV while the cathode work function is 3.3 eV. The mobility parameters of each layer in our device were taken as below Table.1 by Ref. [6]. The device temperature is taken as 300 K.

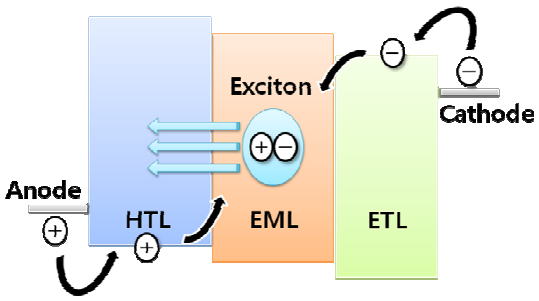

Fig. 1. A schematic diagram of a 3-layer OLED structure with a S-TAD for hole transport layer, a S-DPVBi for emission layer, and a Alq_3 for electron transport layer.

Table 1. The mobility parameters of each layer is listed where μ_0 is zero-field mobility and E_0 is the characteristic field

Material	$\mu_{0,e}$ (cm^2/Vs)	$E_{0,e}$ (kV/cm)	$\mu_{0,h}$ (cm^2/Vs)	$E_{0,h}$ (kV/cm)
HTL	1×10^{-8}	1×10^{5}	4.3×10^{-4}	1×10^{3}
EML	2 x 10-8	11.8	2×10^{-8}	11.8
ETL	1.2×10^{-6}	1959	1×10^{-7}	1959

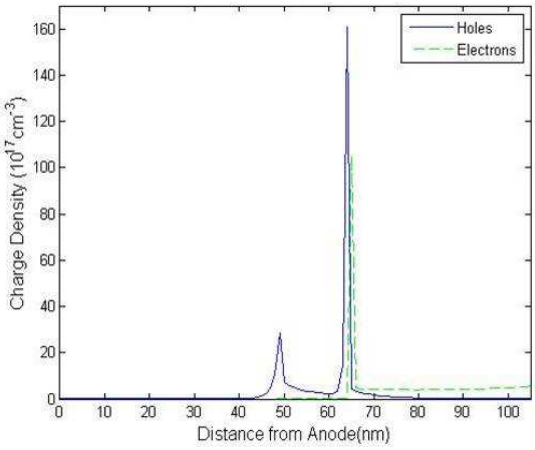

Fig. 2. Simulated profiles of charge carrier densities as a function of the distance from the anode at steady-state. The internal interfaces between the three layers are located at 50 nm and 65 nm away from the anode.

Fig. 2 is a plot illustrating the charge density distribution as a function of the distance from the anode in nanometer scale when 10 V is applied. Fig. 1 implies that the holes are accumulated at both interfaces of the emission layer and penetrate into the neighboring layers. In the meanwhile, electrons appear to accumulate at the interface between the ETL (Alq_3) and the emission layer (S-DPVBi) and diminish at the adjacent layers. The peak of the curve represents the presence of accumulated electrons high electric field which implies the rapid change of the electric field. Referring to Fig. 2, we can see that the hole concentration decreases in the ETL which implies the space charge limited region for the balance of charge transport. For the similar reason, the electron concentration increases as approaching the cathode.

Fig. 3 is a plot illustrating the densities of exciton (solid line; left axis) and recombination rates (dotted line; right axis) as a function of the distance from the anode. Since the electron and hole concentration exhibits peak at the interface between the emission layer and ETL, the recombination rates also reaches the maximum at this

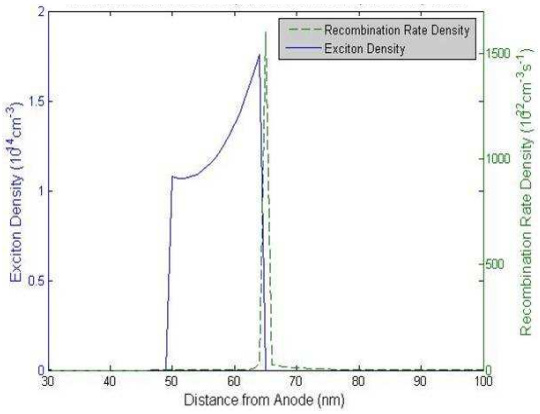

Fig. 3. Simulated profiles of exciton densities and recombination rate as a function of the distance from the anode at steady-state.

interface. Referring to Fig. 3, we can recognize that the recombination rate (dotted line) rapidly increases at the interface. Since the exciton is formed after the electron-hole recombination, we can confirm from Fig. 3 that the exciton concentration also strikes the peak at the interface. Fig. 3 illustrates that the exciton distributes over the emission layer and decreases as approaching the anode.

Fig. 4(a), 4(b), and 4(c) are plots illustrating the transient behavior of the hole, electron, and excitons, respectively, for the OLED structure. The transient analysis is dependent on the position of the charge accumulation and each charge distribution. The amount of space charge is determined by the internal energy barrier while the internal charge density seems to be determined by the barrier height of the injection electrode.

Our FEM study revealed how the recombination density and charge density vary with the thickness of the layer. Now, we will investigate what happens if we insert the EML in bilayer structure. Fig. 5 is a schematic energy band diagram for the comparison. Device A is a basic two-layer structure (ETL and HTL), while Device B and Device C are three-layer structures with EML inserted. In Device B, the LUMO level of the EML aligns with the LUMO of the ETL while the HOMO level of the EML aligns with the HOMO of the HTL. In Device C, the LUMO level of the EML aligns with the LUMO of the HTL while the HOMO level of the EML aligns with the HOMO of the ETL. Here, we compare the electrical properties of these devices.

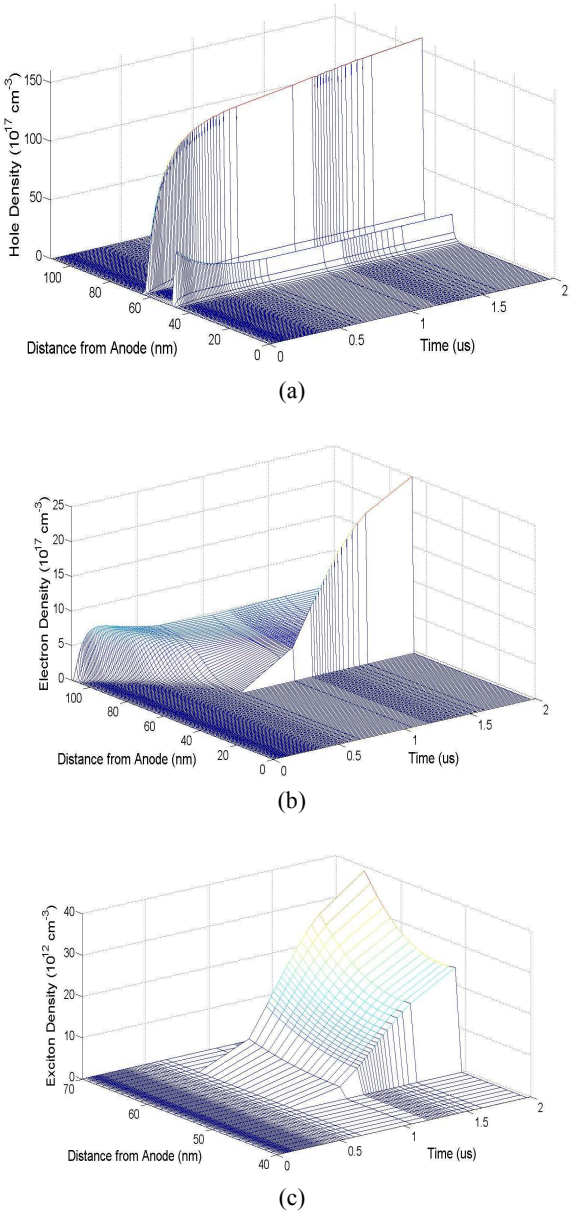

Fig. 4. (a) A plot of the simulated hole density profile in multilayer OLED after turn-on, (b) A plot showing the calculated electron density profile in multilayer OLED as a function of time after turn-on, (c) A plot of calculated transient internal exciton density profiles in a blue-emitting multilayer OLED device.

In Fig. 6(a), we can see that the electric field distribution in the device A, B and C. This plot implies that the recombination occurs mainly at the interface between HTL and ETL in device A. In case of device B, the field stretches out over the EML. In case of device C, however, the peak field is located at the interface between EML and ETL, which implies that the recombination occurs primarily in this region. Fig. 6(b)

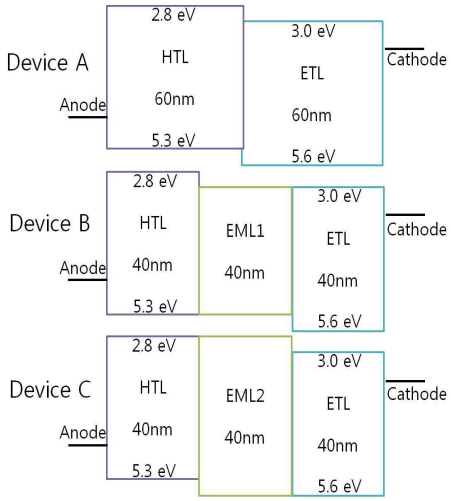

Fig. 5. Schematic energy band diagram for structures: Device A is a basic two-layer structure and Device B and Device C are a three-layer structure with emission layer inserted.

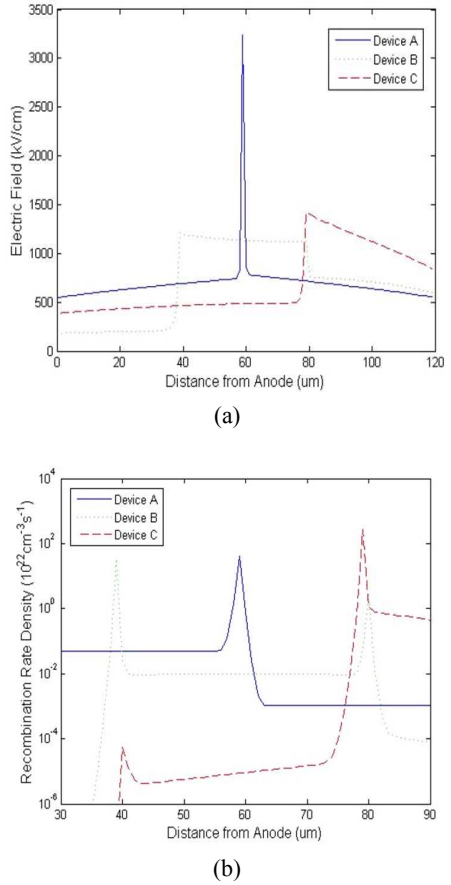

Fig. 6. (a) A plot of calculated distribution of electric field in device A, B and C, (b) A plot illustrating the calculated distribution of recombination rate density in devices A, B and C.

supports our speculations. In device B, the recombination occurs at both edges of the EML. Referring to Fig. 5, the

reason seems to be due to the accumulation of holes and electrons that could not cross the barrier, which means the energy gap between EML1 and HTL for electrons, or the one between EML1 and ETL for holes. This explanation is confirmed by the results shown in Fig. 7(a), 7(b), and 7(c).

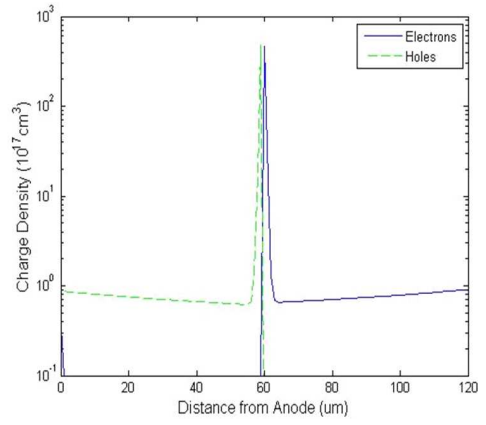

(a)

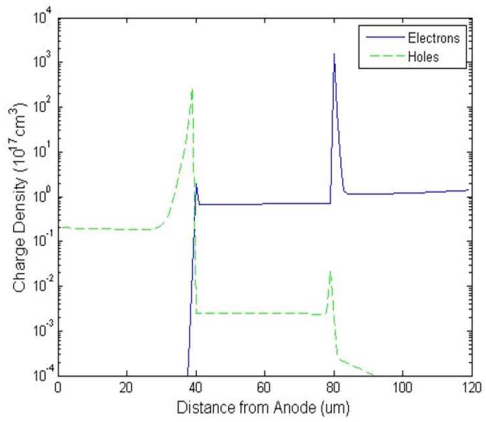

(b)

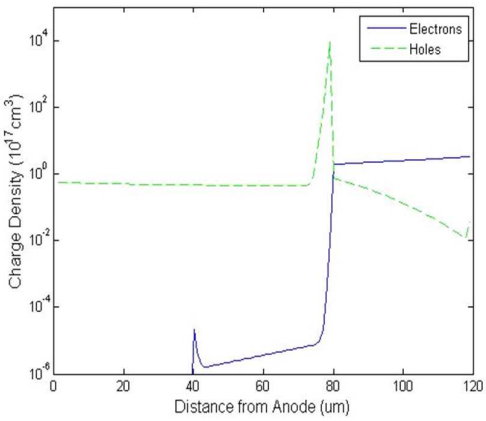

(c)

Fig. 7. (a) Simulated profiles of carrier charge density in device A, (b) Simulated profiles of carrier charge density in device B, (c) Simulated profiles of carrier charge density in device C.

Fig. 7(a), 7(b), and 7(c) exhibit the profiles of carrier density for eacj of devices A, B, and C, respectively. The accumulation of carriers occurs between two layers in the bilayer device A. Since the carrier mobility of each layer is about the same, the density is symmetrical on the axis of interface. In the trilayer device B, the electrons which do not incline the energy gap between EML1 and HTL are accumulated at the edge of EML1. Similarly, the holes are accumulated at the other edge of EML1. However, in device C, electrons and holes are recombined at the interface of EML2 and ETL. The reason why the density of holes is higher than that of electrons seems to be that the mobility of holes is higher than that of electrons in the EML2. Since fast holes arrive at the recombination region earlier, the electrons vanish when they arrive. Therefore the density of the holes and recombination rate density exhibit the peak in this area, as can be seen in Fig. 6(b) and Fig. 7(c).

IV. SUMMARY

We report our numerical study on the space charge effects at the interface for OLED structure with basis on tris (8-hydroxyquinolinato) aluminum (Alq_3). The physical model covers all the key physical processes in OLEDs, namely charge injection, transport and recombination, exciton diffusion, transfer and decay as well as light coupling, and thin-film-optics. The exciton model includes generation, diffusion, and energy transfer as well as annihilation. Our simulation results investigated the accumulation of charges at internal interfaces and their signature in the transient response as well as the electric field distribution for space charge effects. We also discussed that the effect of the insertion of the EML in bilayer structure. Unlike bilayer structure, in trilayer device, electrical properties are more susceptible to the HOMO and LUMO energy level of emission layer. Further investigations will be made for understanding the influence of traps and doping concentration on the device properties.

ACKNOWLEDGEMENTS

This work was supported by INHA University Research Grant.

REFERENCES

[1] B. Ruhstaller *et al.*, "Transient and steady-state behavior of space charges in multilayer organic light-emitting diodes", *J. Appl. Phys.*, vol. 89, pp. 4575-4586, 2001.

[2] Editor-in-chief, David R. Lide; associate editor, H.P.R. Frederiksse, *CRC handbook of chemistry and physics*, Boca Raton; New York: CRC Press, 1997.

[3] Chan-Ching Chang, Ming-Ta Hsieh, Jenn-Fang Chen, Shiao-Wen Hwang, and Chin H. Chen, "Highly power efficient organic light-emitting diodes with a p-doping layer", *J. Appl. Phys. Lett.* 89, 253504, 2006.

[4] Dexter D. L., "Theory of Sensitized Luminescence in Solids", J. Chem. Phys. vol. 21, pp. 836-850, 1953.

[5] Beat Ruhstaller, Evelyne Knapp, Benjamin Perucco, Nils Reinke, Daniele Rezzonico and Felix Muller, "Advanced Numerical Simulation of Organic Light-emitting Devices", Optoelectronic Devices and Properties, 21, 2011.

[6] U. Bach et al., "Characterization of hole transport in a new class of spiro-linked oligotriphenylamine compounds", Adv. Mater., vol. 12, pp. 1060-1063, 2000.

Kwang-sik Kim was born in Jeju Island, Korea, in 1989. He received the B.A degree in Electrical Engineering from Inha University in 2011. His current research interests include the numerical analysis of organic light-emitting diodes.

Young-Wook Hwang was born in Icheon, Korea, in 1987. He received the B.A degree in Electrical Engineering from Inha University in 2012. His current research interests include the numerical analysis of organic light-emitting diodes.

Tae-Young Won received the M.A degree in Electronic Engineering from Korea Advanced Institute of Science and Technology in 1983 and the Ph.D degree from University of Illinois at Urbana- Champaign. In recent years, he has started research on the numerical analysis of organic light-emitting diodes.